

## New progress of plasmonics in complex metal nanostructures

TIAN XiaoRui, TONG LianMing & XU HongXing\*

*Beijing National Laboratory for Condensed Matter Physics, Institute of Physics, Chinese Academy of Sciences, Beijing 100190, China*

Received September 16, 2013; accepted October 31, 2013; published online November 14, 2013

Noble metal nanostructures possess novel optical properties because of their collective electronic oscillations, known as surface plasmons (SPs). The resonance of SPs strongly depends on the material, surrounding environment, as well as the geometry of the nanostructures. Complex metal nanostructures have attracted research interest because of the degree of freedom in tailoring the plasmonic properties for more advanced applications that are unattainable by simple ones. In this review, we discuss the plasmonic properties of several typical types of complex metal nanostructures, that is, electromagnetically coupled nanoparticles (NPs), NPs/metal films, NPs/nanowires (NWs), NWs/NWs, and metal nanostructures supported or coated by dielectrics. The electromagnetic field enhancement and surface-enhanced Raman scattering applications are mainly discussed in the NPs systems where localized SPs have a key role. Propagating surface plasmon polaritons and relevant applications in plasmonic routers and logic gates using NWs network are also reviewed. The effect of dielectric substrates and surroundings of metal nanostructures to the plasmonic properties is also discussed.

**surface plasmons, complex metal nanostructures, SERS, plasmonic router, logic gates, Fano resonance**

**PACS number(s):** 78.67.-n, 81.07.-b, 81.05.-t

**Citation:** Tian X R, Tong L M, Xu H X. New progress of plasmonics in complex metal nanostructures. *Sci China-Phys Mech Astron*, 2013, 56: 2327–2336, doi: 10.1007/s11433-013-5339-3

### 1 Introduction

Because of the unique optical properties, plasmonics has become one of the most interesting and active research areas in nanotechnology [1–6]. In metal nanoparticles (NPs), the collective oscillations of free electrons are confined in all three-dimensions, resulting in the reputed localized surface plasmons (LSPs). Once excited, LSPs produce large electromagnetic (EM) field enhancement around the surface of NPs, which has been widely used in surface-enhanced spectroscopies [7], optical forces [8,9], catalysis [10,11], etc. The LSPs resonance (LSPR) is extremely sensitive to the dielectric environment, leading to a series of LSPR sensing techniques [12,13]. In metal thin films and nanowires (NWs), the electrons are free to move in one or two dimen-

sions, thus propagating surface plasmon polaritons (SPPs) can be excited and propagate along the metal/dielectric interface. The propagating characteristics of SPPs have found many important applications including plasmonic routers, logic gates and optical circuits [14,15].

Although the optical properties of single metal nanostructures have already been extensively studied [16–19], more tunable SPs and more advanced applications can be achieved by assembling single objects into complex nanostructures [20–22]. In the simplest case, when two metal NPs are placed in close proximity to each other, the plasmon modes in one NP couple strongly with those in the other, and as a result, new hybridized plasmon modes are formed and extra EM enhancement is obtained at the gap [23–27]. The strength of the near-field coupling is strongly determined by the gap distance, the excitation wavelength and polarization [28,29].

Herein we will discuss our recent progress of plasmonics

\*Corresponding author (email: hongxingxu@iphy.ac.cn)

in several typical types of complex metal nanostructures, including NPs aggregates, NPs on metal film, coupled NPs/NWs, NWs/NWs, and metal nanostructures supported and/or coated by dielectric layers. The EM coupling and Raman enhancement at the nanogaps between NPs, NPs/NWs, and NPs/metal film will be discussed. For metal NWs, the characteristics of propagating SPPs and applications such as plasmonic routers and logic gates will be reviewed. Since the dielectric substrate and surroundings drastically affect the resonance of SPs, we will also discuss NPs or NWs supported and/or coated by dielectric layers and define it as a special type of metal-dielectric nanostructures.

## 2 Coupled metal NPs

### 2.1 NPs dimers and “hot spots”

The EM coupling effects in NPs dimers have been intensively studied [30–32]. The theory of plasmon hybridization developed by Prodan et al. [33] provides an intuitive physical picture of how the plasmon modes are coupled. If the incident electric field is parallel to the axis of a dimer of identical NPs, the near-field coupling is much stronger than that under perpendicular polarization. The gap distance is another crucial parameter that determines the coupling. With decreasing gap distance, the energy of the longitudinal plasmon mode is lowered and the resonance peak redshifts. The quantitative description of the redshift can be measured using the reputed plasmon ruler [34–36]. For the dimers composed of two different NPs, that is, heterodimer, the SP modes can be out of phase in the two particles, and novel optical properties such as Fano resonance can arise [37]. The EM coupling between non-spherical NPs also depends on the relative orientation of the two NPs [38,39].

The EM coupling in a dimer results in huge EM field enhancement at the nanogap. Figure 1 gives the near-field plot around a dimer of 90 nm Ag NPs with 5.5 nm gap distance excited by 514.5 nm laser at different polarization angles. It can be seen that the induced EM field is concentrated at the gap, and the magnitude is the strongest if the incident electric field is parallel to the dimer axis (Figure 1(a)), whereas it is almost identical as that of a single NP if the polarization is orthogonal.

The nanogaps which strongly confine induced EM fields are supreme systems for SERS applications. Various types of nanogaps have been developed for SERS, for example, in nanohole or NPs arrays [40,41], nanohole/NP pairs [42], nanocube dimers [43] and nanorod dimers [44]. Indeed, the nanogap effect has impacted, and to some extent, given rise to, a series of interesting topics in plasmonics, including not only single molecule SERS [45–47], but also plasmonic antennas [48], plasmonic tweezers [8,9], quantum plasmonics [49–52], and nonlinear plasmonics [53,54].

The field enhancement at the nanogap of a dimer with

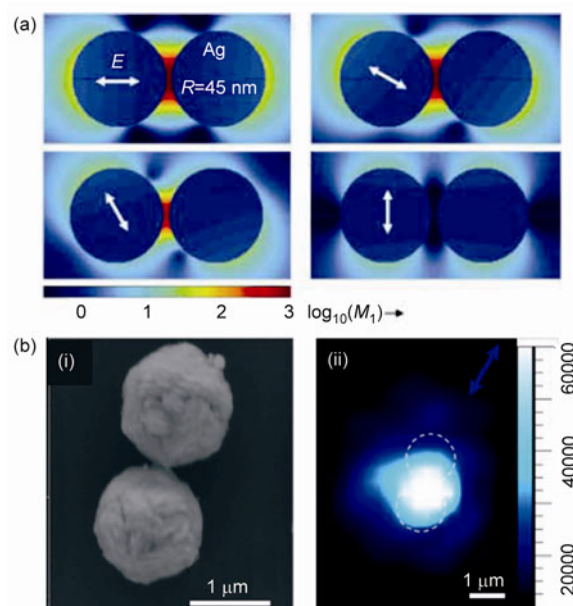


**Figure 1** (a) Near-field plots of a dimer of Ag NPs (gap distance 5.5 nm) at different excitation polarization angles (arrows indicate the excitation polarizations). Excitation wavelength: 514.5 nm. Reprinted from ref. [55]. (b) SEM image of flower-like mesoparticle dimer of Ag (left) and the corresponding SERS image (arrow indicates the excitation polarization). Reproduced elsewhere [56].

certain separation can be further improved if the surfaces of the particles are roughened rather than smooth. Recently, Liang et al. [56] reported enormous SERS enhancement ( $\sim 10^{10}$ ) from dimers of chemically synthesized flower-like Ag mesoparticles. The flower-like Ag mesoparticles are approximately one micrometer in diameter, and can be conveniently manipulated with a micro-probe under a conventional optical microscope. Figure 1(b-i) shows a typical SEM image of a dimer created by micro-manipulation. The corresponding SERS image in Figure 1(b-ii) indicates that “hot spot” is formed at the gap when the excitation polarization is parallel to the dimer axis (indicated by the blue arrow). The polarization dependent SERS images evidenced that the strong EM field in the gap is also a result of the interparticle coupling.

### 2.2 Oligomers of NPs

The EM coupling in oligomers of NPs, the reputed “plasmonic artificial molecules”, is more complex than that in dimers [57–60]. It is worth noting that, in symmetric oligomers, the plasmonic modes can be qualitatively analyzed according to group theory [61–63].

Fano resonance, arising from the coherent coupling and interference of continuum-like broad super-radiant modes and narrow subradiant modes [64], is a typical consequence of EM coupling in oligomers. This coupling can be tuned straightforwardly by changing the geometry and composition. For example, Lassiter et al. [65] reported strong Fano

resonances in heptamers. In such a cluster, the Fano resonance is a result of the interference between a bonding bright (superradiant) mode where the dipolar plasmons of all NPs oscillate in phase and in the same direction, and an antibonding dark (subradiant) mode, where the dipole moment of the center particle opposes the dipole moment of the surrounding ring. Moreover, the resonance wavelength and amplitude can be sensitively tuned by altering the cluster dimensions, geometry, and relative size of the individual NPs. For simple oligomers such as trimers and quadrumers, the subradiant modes do not exist, thus the symmetry needs to be broken in order to obtain Fano resonance [66].

### 3 Coupled NPs/metal film and NPs/NWs

#### 3.1 NP over metal film (NPOF)

A dipole on the surface of a substrate induces an image dipole in the substrate, and interacts with it if the incident electric field has a component perpendicular to the surface. A metal NP on a metal film is such a system: the NP couples to the image electromagnetically, and the resonance of LSP in the NP is altered [67–70]. An important fact is that the metal film supports propagating plasmons, that is, SPPs, which also alter the NP plasmon resonance depending on the relative energies of the LSPs and SPPs. Moreover, the interaction strongly depends on the distance between the NP and the substrate, which can be controlled using molecule linker [71], thin dielectric shell [72] or atomic-layer-deposited (ALD) dielectric spacer [73].

The EM coupling between the NP and the image particle is in fact similar as the coupling between two real NPs, producing large field enhancement in the gap between the NP and the film. Mubeen et al. [73] systematically studied

the optical responses of gold NPs separated from a thick gold film by an ultrathin oxide. Figures 2(a)–(c) show the schematic and cross sectional high-angle annular dark field scanning transmission electron microscopy (HAADF STEM) images of Au NP near a gold film separated by a thin dielectric spacer deposited using ALD technique. Both the experiment and simulation showed that the maximum SERS enhancement occurs when the incident angle (defined in Figure 2(d)) is  $60^\circ$ , different from that in NP dimer case. This is because the EM field at a given point above the film is a coherent superposition of the incident EM field and that reflected from the surface. The phase difference between the two EM fields determined that there exists an optimized incident angle for maximum SERS. In addition, detailed study shows that the SERS intensity is sensitive to the dielectric constant and the thickness of the oxide spacer layer.

It is important to note that the above mentioned “image particle” picture only holds in cases where the thickness of the film is much larger than the diameter of the NP and the film can then be treated as a mirror. For thin metal film, the interaction between the LSPs of the NP and the non-localized continuum plasmons of the underlying metal film is similar to that between localized electronic states with a continuum of delocalized electronic states, that is, the band structure of a metal, which can be described using EM analog of the spinless Anderson-Fano model [74]. This type of interaction may give rise to interesting phenomenon—resonant particle-film virtual state [75].

#### 3.2 Coupled NPs/NWs

Metal NWs have attracted research focus in recent years [76–79]. Because of the one-dimensional geometry of the NWs, light can be coupled in, confined at subwavelength scale, propagates along the NW, and re-emit remotely. The

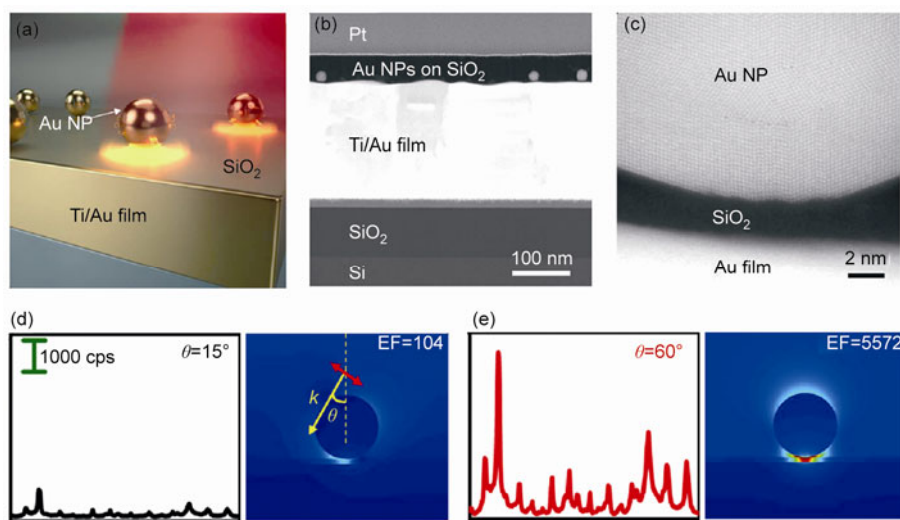


**Figure 2** (a) Schematic and (b) cross sectional HAADF STEM images of Au-NP near a gold film separated by a thin dielectric spacer deposited using ALD technique. (c) High-resolution TEM image of an individual Au-NP on a 2 nm SiO<sub>2</sub> spacer showing its clear separation from the underlying gold film. (d), (e) Measured SERS spectra and it is corresponding calculated EM field distribution and enhancement factors for a gold NPOF with 3 nm SiO<sub>2</sub> thickness, with incident angles of  $15^\circ$  (d) and  $60^\circ$  (e). Reproduced elsewhere [73].

SPP characteristics in metal NWs have been intensively investigated, including the excitation and propagating of multiple SP modes [17,80], the emission directionality at the NW terminals [81,82], the correlation between incident and emission polarizations [83], the effect of substrates and bending on the propagating losses [84]. Vast applications have also been demonstrated, for example, in remote excitation of SERS and fluorescence [85,86], NWs-based plasmonic routers, modulators, and all-optical Boolean logic gates [66,87–89]. Some recent reviews can be referenced elsewhere [14,15]. Note that for practical applications, chemically synthesized metal NWs are usually preferred because of their single-crystalline property and thus low propagation loss.

For a smooth metal NW, SPP can be excited by focusing light at one of the end, or via evanescent field under total internal reflection, and emits at the distal end. At the mid-section, light cannot be coupled into metal NWs directly, and vice versa, coupled out, because of the momentum mismatch between incident photons in dielectric medium and SPPs at metal/dielectric interface. However, if discontinuities are created, for example, a metal NP is moved in proximity to a NW, SPP can be efficiently coupled out/in via scattering. Thus, the coupling between the NW and NP can generate a hot spot in the gap, enabling remote SERS. Figures 3(a) and (b) show the SEM and optical images of a Ag NW-NP structure on a glass substrate [85]. When the laser is focused on the left terminal of the NW, SPPs can be launched, propagate along the NW, and emit from the other terminal, as shown in Figure 3(c). The arrow indicates the polarization of the laser. At the NP/NW junction, SPPs are scattered out and couple to the NP, resulting in an intense EM field that triggers Raman enhancement of the molecules adsorbed therein. Figures 3(d)–(h) show the remote SERS

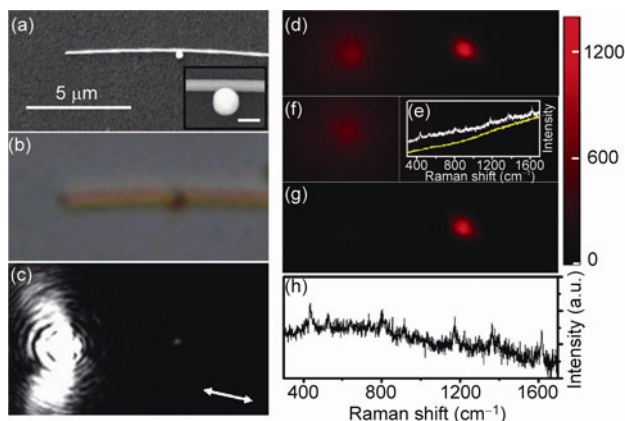


**Figure 3** Remote SERS. (a) SEM image of nanowire-nanoparticle system. (b) Bright field optical image. (c) Optical image collected with a cooled CCD detector and 0.1 s integration time. (d) Raman image at the Stokes peak of  $436\text{ cm}^{-1}$ . (e) Raman spectra from the laser spot at the left end (yellow) and remote wire/particle junction (white). (f) Fluorescence background image. (g) Raman image after background subtraction. (h) Remote-excitation SERS spectrum. Reprinted elsewhere [85].

images and corresponding spectra.

If the laser directly illuminates the NP-NW junction, the EM coupling between the NP and NW is, to some extent, similar to that in the NP/metal film structure [21]. When the excitation polarization is orthogonal to the NW, the localized NP plasmons couple strongly to the continuous NW plasmons, thus dramatically enhanced EM field can be generated in the junction leading to pronounced Raman enhancement, as shown in Figures 4(a) and (b) [90]. The strength of the EM coupling and the Raman enhancement were shown to be insensitive to the detailed shape of the NPs, explained by the plasmon hybridization model. Both the experiment and the simulation show that the enhancement is much weaker when the polarization is parallel to the NW because the induced charges in the NP are distal from the NW than that in the orthogonal case. Detailed study on polarization dependence shows that the SERS intensity has a  $\cos^2\theta$  dependence on the laser polarization, where  $\theta$  is the angle between the polarization direction and the axis orthogonal to the nanowire (Figure 4(c)). Although the Raman enhancement factor is proportional to the fourth power of the electric field enhancement, in the NP/NW coupled structure, only the excitation field enhancement depends on the incident polarization, and the direction of the induced EM field is always across the junction. Therefore, the total SERS enhancement shows  $\cos^2\theta$  dependence, instead of  $\cos^4\theta$  dependence.

## 4 NWs network structures

### 4.1 SPP routing in branched NWs

Branched NWs can be obtained using micromanipulation, as shown in Figure 5(a). When excited at the terminal 1, the plasmons launched along the main wire can also couple and propagate along the branched wire. The launched SPs can be routed to outputs 2 or 3 in a controlled way by modifying the input polarization angle at terminal 1 [66]. Different excitation wavelengths can be routed selectively to either of the outputs by changing polarization (Figures 5(b) and (c)). When 633 nm and 785 nm lasers are focused on wire end 1 simultaneously with a polarization of  $40^\circ$ , the 633 nm light is almost completely routed to the branch wire (output 2) while the 785 nm light is primarily routed in the main wire (output 3). This can be explained by the finite element method (FEM) simulations shown in Figure 5(e). SPP propagates with maximum and minimum amplitudes along the NW. If the branch NW contacts the main wire at a position where the maximum is, SPP is coupled to and propagates along the branch wire rather than the main wire. If the contact point lies in a minimum, the branch wire does not play any role and the SPP propagation along the main wire is not disturbed.

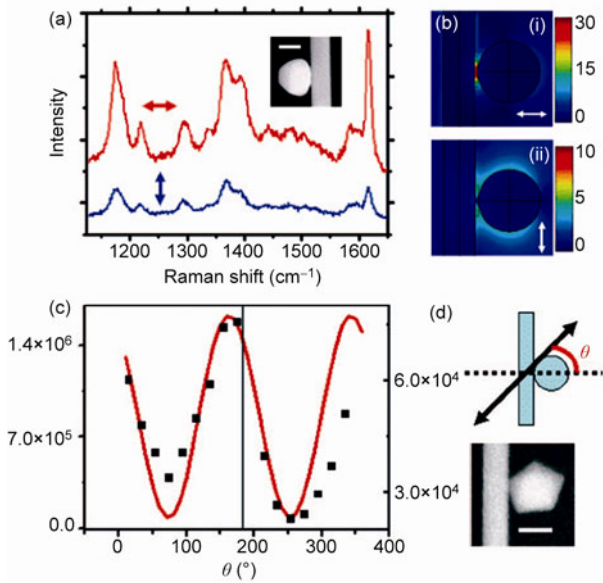


**Figure 4** (a) SERS spectra of MGITC at two different polarizations for the NP/NW structure shown in the inset. (b) Calculated electric field for a gold sphere of radius 50 nm at 5 nm from a wire of radius 25 nm for incident polarization perpendicular (i) and parallel (ii) to the wire. (c) Measured (squares) and calculated (lines) SERS intensity as a function of polarization angle  $\theta$  defined in (d). (d) Definition of the angle  $\theta$  and SEM image of the wire-particle system in (c). The scale bar in the SEM images is 200 nm. Reproduced elsewhere [90].

#### 4.2 SPP interference in complex NWs network

The SPP routing can be used for plasmonic devices, for example, logic gates in specially designed complex NWs networks. Figure 6(a) gives a NWs network composed of a main wire (the longest one) and two branch wires, including two inputs (I1 and I2) and two outputs (O1 and O2). SPPs can be launched in the main and branch NWs simultaneously through I1 and I2, and interfere with each other at the junction. The interference can be modulated by changing the phase difference between the two incident beams. The emissions at either output O1 or O2 can thus be tuned accordingly (Figure 6(b)). For certain relative phases, SPP can be routed selectively to output O1 or output O2 (Figure 6(b)). The mechanism can be revealed intuitively from the QD emission images in Figure 6(c). The QDs emission basically reflects the near-field distribution along the NWs. The output from O2 is controlled by the intensity of the field in the wire junction (dashed yellow rectangle in Figure 6(c)). When the near-field intensity in the junction is weak, the energy propagates to terminal O1 (Figure 6(c-i)). When the intensity in the junction is strong, most of the energy is switched to the branch wire and guided to terminal O2 (Figure 6(c-iii)). For the two incident polarizations indicated by the red arrows in Figure 6(a), the emission intensities from O1 and O2 over several cycles of relative phase ( $2\pi$ /cycle) of the two inputs is shown in Figure 6(d), which shows that the interference between the SPPs generated at I1 and I2 is almost ideal. The interference behavior here can

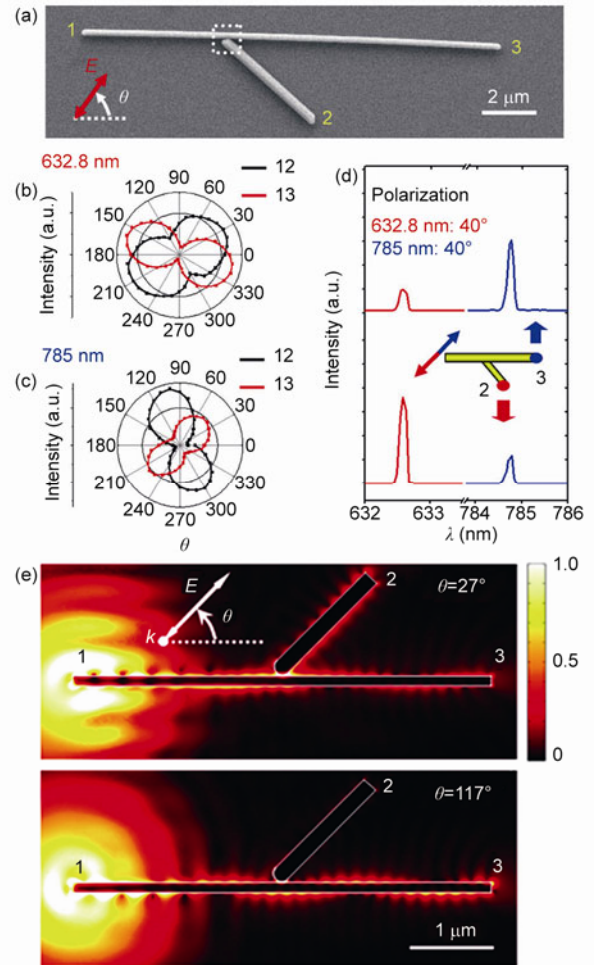


**Figure 5** (a) SEM image of a branched Ag NW structure. (b), (c) Emission intensity from NW end 2 (black) and 3 (red) as a function of incident polarization angle for 633 nm and 785 nm wavelength excitation. (d) Spectra collected from wire end 2 (lower curves) and 3 (upper curves). Polarization angle of the incident light is  $40^\circ$ . (e) FEM simulated local electric field distributions for maximal ( $\theta = 27^\circ$ ) and minimal ( $\theta = 117^\circ$ ) emission from the branch wire. Reproduced elsewhere [66].

not be achieved only by controlling the excitation polarization.

By defining certain intensity values as thresholds, the strong and weak output intensity can be assigned as “ON (or 1)” and “OFF (or 0)” states, and the NW structures can realize certain logical operations. For example, for an intensity threshold of 450 au, and considering O2 as the output, (I1 = ON, I2 = OFF) results in O2 = OFF, (I1 = OFF, I2 = ON) results in O2 = OFF, and (I1 = ON, I2 = ON) input results in O2 = ON, demonstrating the behavior of an AND gate. By considering O1 as another output, this NWs network can be used as a binary half adder [87].

Based on the SPPs interference principle, a complete set of plasmonic logic gates and other functional devices can be realized by designing different NW networks [88,91].

## 5 Metal-dielectric nanostructures

As mentioned above, the dielectric substrate and surround-

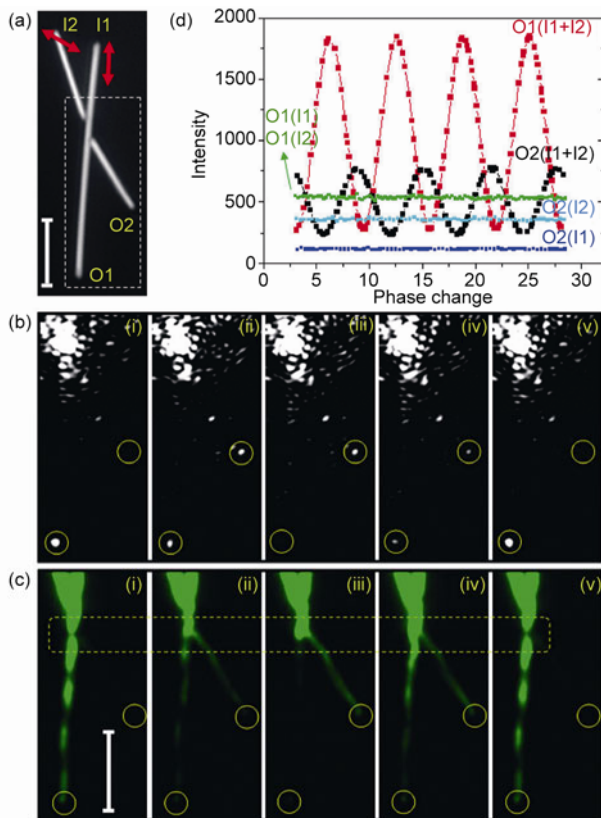


**Figure 6** Interference of plasmons in Ag NWs. (a) Optical image of the network. (b) Scattering images for two beam interference in one cycle. (c) QD emission images in one interference cycle. (d) Scattering intensity at O1 and O2 terminals. Red, the intensity of O1 for simultaneous input of both I1 and I2; black, the intensity of O2 for simultaneous input of I1 and I2; green, the intensity of O1 for I1 only and I2 only; cyan, the intensity of O2 for I2 only; blue, the intensity of O2 for I1 only.  $\text{Al}_2\text{O}_3$  thickness is 50 nm, scale bar is 5  $\mu\text{m}$ . Red arrows in (A) show the polarization of the two laser beams, and the white dashed rectangle in (a) mark the area displayed in (b) and (c). Reprinted from ref. [87]

ings dramatically affect the SPs properties of the metal nanostructures. Metal-dielectric composites typically refer to core-shell NPs, that is, metal@dielectric and dielectric@metal hybrids. The existence of dielectric components changes the optical response of metal nanostructures. Some insulator compounds (such as  $\text{VO}_2$ ,  $\text{WO}_3$ , S<sub>m</sub>S) can even undergo metal-insulator transition and possess novel optical properties [92–94]. Reviews articles have systematically summarized such interesting properties [19,95,96]. Metal nanostructures supported by dielectric substrates or coated by dielectric films, by absolute definition, not composites, however, as the dielectric substrate or coating dramatically tunes the optical properties of metal nanostructures, we define them as a special type of metal-dielectric nanostructures and explore the effects of dielectrics in tailoring the SP resonances.

### 5.1 Substrate induced SP modes hybridization

Understanding the EM interactions between plasmonic no-

ble metal nanocrystals and different substrates is critical because a number of plasmon-based devices and applications, such as chemical and biological sensing, subwavelength waveguides and plasmon-enhanced photovoltaic cells, require the attachment of metal nanocrystals onto various substrates [87,97–99]. The presence of the substrate breaks the symmetry of the nanostructure environment and could have a strong influence on the modes of the nanostructure. Figure 7 shows a nanocube placed on a dielectric substrate. The induced charge distribution in the dielectric substrate mediates the coupling of primitive plasmon modes ( $D^0$  and  $Q^0$ ), since the charges of these two modes distributes at the bottom surface of the cube, as shown in Figure 7(a). The coupling of the two modes forms hybridized bonding (D) and antibonding (Q) modes, as shown in Figure 7(b). Because the primitive quadrupolar mode is dark, the interference of the dark mode with the continuum bright dipole mode gives a Fano resonance, which can also be sensitively tuned by changing the distance between the cube and the substrate, as well as by altering dielectric substrates [100].

The above coupling scenery is similar for a NW placed on dielectric substrate. Figure 7(c) shows schematically how several lowest primary SPP modes interact with each other via the dielectric substrate. It can be seen that the otherwise degenerate  $\text{HE}_{\pm 1}$  modes interact predominantly with different primary wire modes and produce a new set of hybrid-

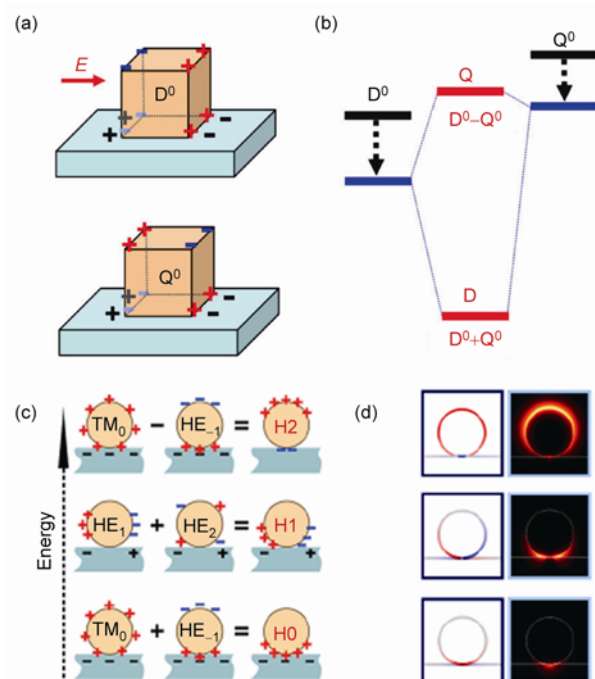


**Figure 7** (a) Schematic illustrating the substrate-mediated  $D^0$  and  $Q^0$  interaction. (b) Energy diagram showing the substrate effect: pure dielectric screening effect (dashed black) which causes red shifts of both modes and the substrate-mediated interaction (thin blue line) resulting in hybridized bonding D and antibonding Q modes. (c) Schematic drawing of how different primary wire plasmons interact through the dielectric substrate. (d) Normalized surface charge contour (left) and time-averaged power flow (right) of the three hybridized modes. Nanowire ( $R = 100 \text{ nm}$ ) is supported on a glass substrate. Reproduced elsewhere [100,101].

ized modes ( $H_0$ ,  $H_1$  and  $H_2$ ). The interaction between the primary  $TM_0$  and  $HE_{-1}$  mode introduces the new fundamental mode  $H_0$ . It is readily apparent that  $H_0$  mode is primarily localized at the bottom, which can be used for sub-wavelength plasmonic waveguiding and used in various deep sub-wavelength active devices such as electro-optical or all-optical modulators. However, for substrates with a high permittivity,  $H_0$  could become leaky when the energy is below a critical value, which will raise the propagating loss [101].

Interactions of  $HE_{\pm 1}$  modes with other different primary wire modes give  $H_1$  and  $H_2$  mode, as shown in Figure 7(c). The  $H_1$  mode comes from an in-phase (inducing the same polarized charges on the substrate surface) coupling of the  $HE_1$  and  $HE_2$  modes, while the  $H_2$  mode comes primarily from an out-of-phase (canceling their induced polarized charges on the substrate surface) coupling between the  $TM_0$  and  $HE_1$  mode. Figure 7(d) shows the calculated surface charges and the time-averaged power flow distributions of the three lowest order hybridized modes. The charge plots are in good agreement with those in Figure 7(c), confirming the understanding of the interactions of different wire plasmons via the substrate. Similarly, the degree of interaction with the substrate can be controlled by changing the nanowire shape, gap, and refractive index of the substrate.

## 5.2 Tuning SPs on NWs using dielectric coating

The plasmon resonances in metal nanostructures are sensitive to the change of surrounding dielectric materials. For one-dimensional metal NWs, the SPP wavelength can be easily tuned by coating dielectric films. Recently, Wei et al. [102] studied the propagating SPs on Ag NWs with differ-

ent thickness of  $Al_2O_3$  coating layer. Figures 8(a) and (b) show the schematic cross section of the sample and the SPP excitation/collection configuration. The QDs images in Figures 8(d) and (e) show that the near-field beat period ( $\Lambda$ ) depends on the thickness of the oxide film and the dielectric medium. Three NWs of similar diameters deposited different thickness of  $Al_2O_3$  film were shown in Figure 8(d). It can be seen that when the thickness of  $Al_2O_3$  increases from 30 nm to 80 nm (top to bottom),  $\Lambda$  dramatically increases from 1.7  $\mu m$  to 5.8  $\mu m$ . Figure 8(e) shows the near-field distributions for a single NW deposited  $Al_2O_3$  of 50 nm (top), 55 nm (middle) and 60 nm (bottom). A high sensitivity of  $\Lambda$  increasing by 90 nm per nanometer increasing of  $Al_2O_3$  is achieved. This high-sensitivity effect can be explained by the effect of coating on the propagation constants and the dispersion curves of NW SPs [102]. The refractive index of the surrounding medium can also dramatically change the near-field  $\Lambda$ . Figure 8(f) shows that when the NW is moved from the air to water and oil,  $\Lambda$  increases dramatically from 1.3  $\mu m$  to 4.4  $\mu m$  (in water) and 7.2  $\mu m$  (in oil). Such high sensitivity is crucial in various applications such as plasmonic routing and demultiplexing, and may pave the way to the development of on-chip ultrasensitive biosensing.

## 6 Conclusion

In complex metal nanostructures, the SPs in each single component interact with that in the others, for example, LSPs in a single NP can couple to that in another one or to SPPs in a NW or metal film, resulting in extra EM enhancement at the nanogaps. SPPs in different NWs can in-

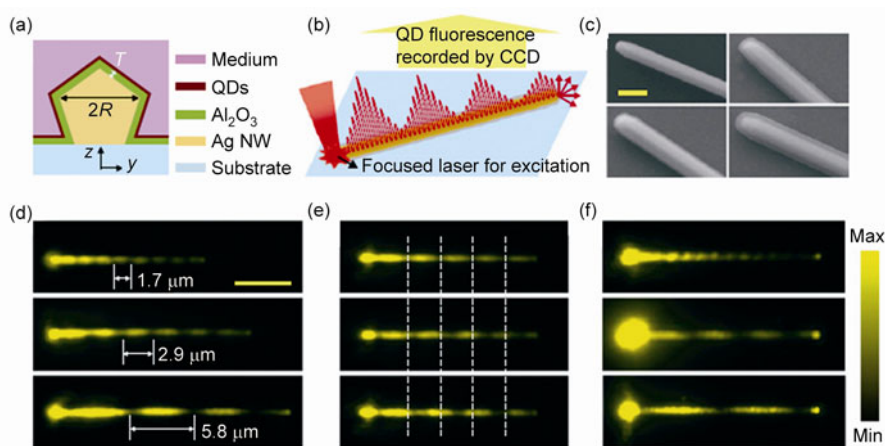


**Figure 8** Near-field distribution images for NWs in different dielectric environments. (a) Schematic cross-section of the sample. (b) Schematic illustration of the excitation/collection configuration and the plasmons propagating along the NW. (c) SEM images of a typical bare Ag NW (upper left) and NWs coated with  $T = 30$  nm (lower left), 50 nm (upper right), and 80 nm (lower right)  $Al_2O_3$  layers. (Scale bar, 500 nm.) (d) QD emission images under excitation at the left ends of the NWs. From top to bottom, the radius of the NWs is 160, 155, and 157 nm, and the corresponding  $Al_2O_3$  thicknesses are 30, 50, and 80 nm. (e) QD emission images for a 162 nm radius NW with a 50 nm  $Al_2O_3$  coating measured in air (top), and then after depositing 5 nm of  $Al_2O_3$  (middle), and finally with an additional 5 nm of  $Al_2O_3$  (bottom). White dashed lines are visual guides to show the shift of the plasmon near-field pattern. (f) QD emission images for a 155-nm radius NW initially coated with 10 nm of  $Al_2O_3$  and QDs, and then capped with another 5 nm of  $Al_2O_3$  to protect the water-soluble QDs from being removed, measured in air (top), water (middle), and oil (bottom). (Scale bar in Figure 8(d) for Figures 8(d)–(f), 5  $\mu m$ .) Reprinted elsewhere [102].

terfere with each other, making possible selective routing of propagating SPPs to desired output terminals. The complex EM interactions give rise to more flexibility in tailoring the SPs for advanced applications, such as remote SERS sensing and plasmonic logic gates. The dielectric substrate or surface coating is another critical parameter that affects the SPs properties, including the LSPR and the SPPs wavelength and propagation length. In fact, this effect provides an alternative method to tailor the SPs characteristics for particular applications.

In general, there still exist many problems to be solved for reliable practical applications of SPs in complex metal nanostructures. For example, the precise control of gap distances between colloidal NPs for reproducible, highly stable and sensitive SERS substrates is still being researched. For future integrated nanophotonic circuits, each necessary component, such as nanoscale light source, plasmonic router and modulator, logic gates, opto/electro converter, is a challenging task currently, aside from the integration of all these components for on-chip devices. However, with the rapid development of micro-fabrication techniques and the further exploration of the plasmonic properties of complex metal nanostructures, future advances addressing these challenges can be anticipated.

*This work was supported by the Ministry of Science and Technology of China (Grant Nos. 2009CB930700 and 2012YQ12006005), the National Natural Science Foundation of China (Grant Nos. 11134013 and 11227407) and the Knowledge Innovative Program of the Chinese Academy of Sciences (Grant No. KJCX2-EW-W04).*

- Gramotnev D K, Bozhevolnyi S I. Plasmonics beyond the diffraction limit. *Nat Photon*, 2010, 4: 83–91
- Atwater H A, Polman A. Plasmonics for improved photovoltaic devices. *Nat Mater*, 2010, 9: 205–213
- Schuller J A, Barnard E S, Cai W S, et al. Plasmonics for extreme light concentration and manipulation. *Nat Mater*, 2010, 9: 193–204
- Shalaev V M. Transforming light. *Science*, 2008, 322: 384–386
- Brongersma M L, Shalaev V M. Applied physics the case for plasmonics. *Science*, 2010, 328: 440–441
- Lal S, Link S, Halas N J. Nano-optics from sensing to waveguiding. *Nat Photonics*, 2007, 1: 641–648
- Moskovits M. Surface-enhanced raman spectroscopy: A brief perspective. *Top Appl Phys*, 2006, 103: 1–17
- Li Z P, Käll M, Xu H. Optical forces on interacting plasmonic nanoparticles in a focused gaussian beam. *Phys Rev B*, 2008, 77: 085412
- Xu H X, Käll M. Surface-plasmon-enhanced optical forces in silver nanoaggregates. *Phys Rev Lett*, 2002, 89: 246802
- Tian X R, Chen L, Xu H X, et al. Ascertain genuine sers spectra of p-aminothiophenol. *Rsc Advances*, 2012, 2: 8289–8292
- Sun M T, Xu H X. A novel application of plasmonics: Plasmon-driven surface-catalyzed reactions. *Small*, 2012, 8: 2777–2786
- Anker J N, Hall W P, Lyandres O, et al. Biosensing with plasmonic nanosensors. *Nat Mater*, 2008, 7: 442–453
- Mayer K M, Hafner J H. Localized surface plasmon resonance sensors. *Chem Rev*, 2011, 111: 3828–3857
- Wei H, Xu H. Nanowire-based plasmonic waveguides and devices for integrated nanophotonic circuits. *Nanophotonics*, 2012, 1: 155–169
- Lal S, Hafner J H, Halas N J, et al. Noble metal nanowires: From plasmon waveguides to passive and active devices. *Accounts Chem Res*, 2012, 45: 1887–1895
- Wei H, Reyes-Coronado A, Nordlander P, et al. Multipolar plasmon resonances in individual ag nanorice. *ACS Nano*, 2010, 4: 2649–2654
- Zhang S P, Wei H, Bao K, et al. Chiral surface plasmon polaritons on metallic nanowires. *Phys Rev Lett*, 2011, 107: 096801
- Zeng H, Sun S H. Syntheses, properties and potential applications of multicomponent magnetic nanoparticles. *Adv Funct Mater*, 2008, 18: 391–400
- Cortie M B, McDonagh A M. Synthesis and optical properties of hybrid and alloy plasmonic nanoparticles. *Chem Rev*, 2011, 111: 3713–3735
- Tong L M, Wei H, Zhang S P, et al. Optical properties of single coupled plasmonic nanoparticles. *Phys Chem Chem Phys*, 2013, 15: 4100–4109
- Halas N J, Lal S, Chang W S, et al. Plasmons in strongly coupled metallic nanostructures. *Chem Rev*, 2011, 111: 3913–3961
- Rycenga M, Cobley C M, Zeng J, et al. Controlling the synthesis and assembly of silver nanostructures for plasmonic applications. *Chem Rev*, 2011, 111: 3669–3712
- Wang H, Brandl D W, Nordlander P, et al. Plasmonic nanostructures: Artificial molecules. *Accounts Chem Res*, 2007, 40: 53–62
- Davis T J, Gomez D E, Vernon K C. Simple model for the hybridization of surface plasmon resonances in metallic nanoparticles. *Nano Lett*, 2010, 10: 2618–2625
- Hentschel M, Saliba M, Vogelgesang R, et al. Transition from isolated to collective modes in plasmonic oligomers. *Nano Lett*, 2010, 10: 2721–2726
- Choi C L, Alivisatos A P. From artificial atoms to nanocrystal molecules: Preparation and properties of more complex nanostructures. *Annu Rev Phys Chem*, 2010, 61: 369–389
- Ye J, Van Dorpe P, Lagae L, et al. Observation of plasmonic dipolar anti-bonding mode in silver nanoring structures. *Nanotechnology*, 2009, 20: 465203
- Zhang Z, Weber-Bargioni A, Wu S W, et al. Manipulating nanoscale light fields with the asymmetric bowtie nano-colorsorter. *Nano Lett*, 2009, 9: 4505–4509
- Jain P K, El-Sayed M A. Plasmonic coupling in noble metal nanostructures. *Chem Phys Lett*, 2010, 487: 153–164
- Huang F M, Baumberg J J. Actively tuned plasmons on elastomericly driven au nanoparticle dimers. *Nano Lett*, 2010, 10: 1787–1792
- Lassiter J B, Aizpurua J, Hernandez L I, et al. Close encounters between two nanoshells. *Nano Lett*, 2008, 8: 1212–1218
- Sheikholeslami S, Jun Y W, Jain P K, et al. Coupling of optical resonances in a compositionally asymmetric plasmonic nanoparticle dimer. *Nano Lett*, 2010, 10: 2655–2660
- Prodan E, Radloff C, Halas N J, et al. A hybridization model for the plasmon response of complex nanostructures. *Science*, 2003, 302: 419–422
- Jun Y W, Sheikholeslami S, Hostetter D R, et al. Continuous imaging of plasmon rulers in live cells reveals early-stage caspase-3 activation at the single-molecule level. *Proc Natl Acad Sci USA*, 2009, 106: 17735–17740
- Reinhard B M, Sheikholeslami S, Mastroianni A, et al. Use of plasmon coupling to reveal the dynamics of DNA bending and cleavage by single ecorv restriction enzymes. *Proc Natl Acad Sci USA*, 2007, 104: 2667–2672
- Sonnichsen C, Reinhard B M, Liphardt J, et al. A molecular ruler based on plasmon coupling of single gold and silver nanoparticles. *Nat Biotechnol*, 2005, 23: 741–745
- Brown L V, Sobhani H, Lassiter J B, et al. Heterodimers: Plasmonic properties of mismatched nanoparticle pairs. *ACS Nano*, 2010, 4: 819–832
- Shao L, Woo K C, Chen H J, et al. Angle- and energy-resolved plasmon coupling in gold nanorod dimers. *ACS Nano*, 2010, 4: 3053–3062
- Tabor C, Van Haute D, El-Sayed M A. Effect of orientation on plasmonic coupling between gold nanorods. *ACS Nano*, 2009, 3: 3670–3678

- 40 García de A F J. Colloquium: Light scattering by particle and hole arrays. *Rev Mod Phys*, 2007, 79: 1267–1290
- 41 Le F, Brandl D W, Urzhumov Y A, et al. Metallic nanoparticle arrays: A common substrate for both surface-enhanced raman scattering and surface-enhanced infrared absorption. *Acs Nano*, 2008, 2: 707–718
- 42 Wei H, Hakanson U, Yang Z L, et al. Individual nanometer hole-particle pairs for surface-enhanced raman scattering. *Small*, 2008, 4: 1296–1300
- 43 Lee S Y, Hung L, Lang G S, et al. Dispersion in the sers enhancement with silver nanocube dimers. *Acs Nano*, 2010, 4: 5763–5772
- 44 Alexander K D, Skinner K, Zhang S P, et al. Tunable sers in gold nanorod dimers through strain control on an elastomeric substrate. *Nano Lett*, 2010, 10: 4488–4493
- 45 Xu H X, Bjerneld E J, Käll M, et al. Spectroscopy of single hemoglobin molecules by surface enhanced raman scattering. *Phys Rev Lett*, 1999, 83: 4357–4360
- 46 Lim D K, Jeon K S, Kim H M, et al. Nanogap-engineerable raman-active nanodumbbells for single-molecule detection. *Nat Mater*, 2010, 9: 60–67
- 47 Xu H X, Aizpurua J, Käll M, et al. Electromagnetic contributions to single-molecule sensitivity in surface-enhanced raman scattering. *Phys Rev E*, 2000, 62: 4318–4324
- 48 Novotny L, van Hulst N. Antennas for light. *Nat Photon*, 2011, 5: 83–90
- 49 Mao L, Li Z P, Wu B, et al. Effects of quantum tunneling in metal nanogap on surface-enhanced raman scattering. *Appl Phys Lett*, 2009, 94: 243102
- 50 Zuloaga J, Prodan E, Nordlander P. Quantum description of the plasmon resonances of a nanoparticle dimer. *Nano Lett*, 2009, 9: 887–891
- 51 Marinica D C, Kazansky A K, Nordlander P, et al. Quantum plasmonics: Nonlinear effects in the field enhancement of a plasmonic nanoparticle dimer. *Nano Lett*, 2012, 12: 1333–1339
- 52 Esteban R, Borisov A G, Nordlander P, et al. Bridging quantum and classical plasmonics with a quantum-corrected model. *Nat Commun*, 2012, 3: 825
- 53 Kim S, Jin J H, Kim Y J, et al. High-harmonic generation by resonant plasmon field enhancement. *Nature*, 2008, 453: 757–760
- 54 Muhlschlegel P, Eisler H J, Martin O J F, et al. Resonant optical antennas. *Science*, 2005, 308: 1607–1609
- 55 Xu H X, Käll M. Polarization-dependent surface-enhanced raman spectroscopy of isolated silver nanoaggregates. *Chem Phys Chem*, 2003, 4: 1001–1005
- 56 Liang H Y, Li Z P, Wang Z X, et al. Enormous surface-enhanced raman scattering from dimers of flower-like silver mesoparticles. *Small*, 2012, 8: 3400–3405
- 57 Quinten M, Kreibig U. Optical-properties of aggregates of small metal particles. *Surf Sci*, 1986, 172: 557–577
- 58 Fan Z Y, Govorov A O. Plasmonic circular dichroism of chiral metal nanoparticle assemblies. *Nano Lett*, 2010, 10: 2580–2587
- 59 Shegai T, Li Z P, Dadosh T, et al. Managing light polarization via plasmon-molecule interactions within an asymmetric metal nanoparticle trimer. *Proc Natl Acad Sci USA*, 2008, 105: 16448–16453
- 60 Urzhumov Y A, Shvets G, Fan J, et al. Plasmonic nanoclusters: A path towards negative-index metafluids. *Opt Express*, 2007, 15: 14129–14145
- 61 Alegret J, Rindzevicius T, Pakizeh T, et al. Plasmonic properties of silver trimers with trigonal symmetry fabricated by electron-beam lithography. *J Phys Chem C*, 2008, 112: 14313–14317
- 62 Brandl D W, Mirin N A, Nordlander P. Plasmon modes of nanosphere trimers and quadrumers. *J Phys Chem B*, 2006, 110: 12302–12310
- 63 Chuntanov L, Haran G. Trimeric plasmonic molecules: The role of symmetry. *Nano Lett*, 2011, 11: 2440–2445
- 64 Fano U. Effects of configuration interaction on intensities and phase shifts. *Phys Rev*, 1961, 124: 1866–1878
- 65 Lassiter J B, Sobhani H, Fan J A, et al. Fano resonances in plasmonic nanoclusters: Geometrical and chemical tunability. *Nano Lett*, 2010, 10: 3184–3189
- 66 Fang Y R, Li Z P, Huang Y Z, et al. Branched silver nanowires as controllable plasmon routers. *Nano Lett*, 2010, 10: 1950–1954
- 67 Hill R T, Mock J J, Urzhumov Y, et al. Leveraging nanoscale plasmonic modes to achieve reproducible enhancement of light. *Nano Lett*, 2010, 10: 4150–4154
- 68 Park W H, Kim Z H. Charge transfer enhancement in the sers of a single molecule. *Nano Lett*, 2010, 10: 4040–4048
- 69 Vernon K C, Funston A M, Novo C, et al. Influence of particle-substrate interaction on localized plasmon resonances. *Nano Lett*, 2010, 10: 2080–2086
- 70 Leveque G, Martin O J F. Optical interactions in a plasmonic particle coupled to a metallic film. *Opt Express*, 2006, 14: 9971–9981
- 71 Mock J J, Hill R T, Degiron A, et al. Distance-dependent plasmon resonant coupling between a gold nanoparticle and gold film. *Nano Lett*, 2008, 8: 2245–2252
- 72 Li J F, Huang Y F, Ding Y, et al. Shell-isolated nanoparticle-enhanced raman spectroscopy. *Nature*, 2010, 464: 392–395
- 73 Mubeen S, Zhang S P, Kim N, et al. Plasmonic properties of gold nanoparticles separated from a gold mirror by an ultrathin oxide. *Nano Lett*, 2012, 12: 2088–2094
- 74 Fano U. Effects of configuration interaction on intensities and phase shifts. *Phys Rev*, 1961, 124: 1866–1878
- 75 Le F, Lwin N Z, Steele J M, et al. Plasmons in the metallic nanoparticle-film system as a tunable impurity problem. *Nano Lett*, 2005, 5: 2009–2013
- 76 Ditlbacher H, Hohenau A, Wagner D, et al. Silver nanowires as surface plasmon resonators. *Phys Rev Lett*, 2005, 95: 257403
- 77 Dickson R M, Lyon L A. Unidirectional plasmon propagation in metallic nanowires. *J Phys Chem B*, 2000, 104: 6095–6098
- 78 Ozbay E. Plasmonics: Merging photonics and electronics at nanoscale dimensions. *Science*, 2006, 311: 189–193
- 79 Maier S A, Atwater H A. Plasmonics: Localization and guiding of electromagnetic energy in metal/dielectric structures. *J Appl Phys*, 2005, 98: 011101
- 80 Liu N, Li Z, Xu H. Polarization-dependent study on propagating surface plasmons in silver nanowires launched by a near-field scanning optical fiber tip. *Small*, 2012, 8: 2641–2646
- 81 Li Z P, Hao F, Huang Y Z, et al. Directional light emission from propagating surface plasmons of silver nanowires. *Nano Lett*, 2009, 9: 4383–4386
- 82 Shegai T, Miljkovic V D, Bao K, et al. Unidirectional broadband light emission from supported plasmonic nanowires. *Nano Lett*, 2011, 11: 706–711
- 83 Li Z P, Bao K, Fang Y R, et al. Correlation between incident and emission polarization in nanowire surface plasmon waveguides. *Nano Lett*, 2010, 10: 1831–1835
- 84 Wang W H, Yang Q, Fan F R, et al. Light propagation in curved silver nanowire plasmonic waveguides. *Nano Lett*, 2011, 11: 1603–1608
- 85 Fang Y R, Wei H, Hao F, et al. Remote-excitation surface-enhanced raman scattering using propagating silver nanowire plasmons. *Nano Lett*, 2009, 9: 2049–2053
- 86 Wei H, Ratchford D, Li X Q, et al. Propagating surface plasmon induced photon emission from quantum dots. *Nano Lett*, 2009, 9: 4168–4171
- 87 Wei H, Li Z P, Tian X R, et al. Quantum dot-based local field imaging reveals plasmon-based interferometric logic in silver nanowire networks. *Nano Lett*, 2011, 11: 471–475
- 88 Wei H, Wang Z X, Tian X R, et al. Cascaded logic gates in nanophotonic plasmon networks. *Nat Commun*, 2011, 2: 387
- 89 Li Z P, Zhang S P, Halas N J, et al. Coherent modulation of propagating plasmons in silver-nanowire-based structures. *Small*, 2011, 7: 593–596
- 90 Wei H, Hao F, Huang Y Z, et al. Polarization dependence of surface-enhanced raman scattering in gold nanoparticle-nanowire systems. *Nano Lett*, 2008, 8: 2497–2502
- 91 Wei H, Xu H X. Controlling surface plasmon interference in

- branched silver nanowire structures. *Nanoscale*, 2012, 4: 7149–7154
- 92 Cortie M B, Dowd A, Harris N, et al. Core-shell nanoparticles with self-regulating plasmonic functionality. *Phys Rev B*, 2007, 75: 113405
- 93 Mott N F, Friedman L. Metal-insulator transitions in  $\text{VO}_2$ ,  $\text{Ti}_2\text{O}_3$  and  $\text{Ti}_{2-x}\text{V}_x\text{O}_3$ . *Philos Mag*, 1974, 30: 389–402
- 94 Tanaka A. On the metal-insulator transitions in  $\text{VO}_2$  and  $\text{Ti}_2\text{O}_3$  from a unified viewpoint. *J Phys Soc Jpn*, 2004, 73: 152–162
- 95 Costi R, Saunders A E, Banin U. Colloidal hybrid nanostructures: A new type of functional materials. *Angew Chem Int Edit*, 2010, 49: 4878–4897
- 96 Zeng H, Sun S H. Syntheses, properties and potential applications of multicomponent magnetic nanoparticles. *Adv Funct Mater*, 2008, 18: 391–400
- 97 Kravets V, Schedin F, Grigorenko A. Extremely narrow plasmon resonances based on diffraction coupling of localized plasmons in arrays of metallic nanoparticles. *Phys Rev Lett*, 2008, 101: 087403
- 98 Pillai S, Catchpole K R, Trupke T, et al. Surface plasmon enhanced silicon solar cells. *J Appl Phys*, 2007, 101: 093105
- 99 Haes A J V D, Richard P. A nanoscale optical biosensor: Sensitivity and selectivity of an approach based on the localized surface plasmon resonance spectroscopy of triangular silver nanoparticles. *J Am Chem Soc*, 2002, 124: 10596–10604
- 100 Zhang S P, Bao K, Halas N J, et al. Substrate-induced fano resonances of a plasmonic: Nanocube: A route to increased-sensitivity localized surface plasmon resonance sensors revealed. *Nano Lett*, 2011, 11: 1657–1663
- 101 Zhang S P, Xu H X. Optimizing substrate-mediated plasmon coupling toward high-performance plasmonic nanowire waveguides. *ACS Nano*, 2012, 6: 8128–8135
- 102 Wei H, Zhang S P, Tian X R, et al. Highly tunable propagating surface plasmons on supported silver nanowires. *Proc Natl Acad Sci USA*, 2013, 110: 4494–4499